Published in final edited form as:
Science. 2017 October 13; 358(6360): . doi:10.1126/science.aam5776.

Influence of El Niño on atmospheric CO_2 over the tropical Pacific Ocean: findings from NASA's OCO-2 mission

A. Chatterjee[1,2,*], **M. M. Gierach**[3], **A. J. Sutton**[4,5], **R. A. Feely**[4], **D. Crisp**[3], **A. Eldering**[3], **M. R. Gunson**[3], **C. W. O'Dell**[6], **B. B. Stephens**[7], and **D. S. Schimel**[3]

[1]Universities Space Research Association, Columbia, MD

[2]NASA Global Modeling and Assimilation Office, Greenbelt, MD

[3]Jet Propulsion Laboratory, California Institute of Technology, Pasadena, CA

[4]NOAA Pacific Marine Environmental Laboratory, Seattle, WA

[5]Joint Institute for the Study of the Atmosphere and Ocean, University of Washington, S WA

[6]Colorado State University, Fort Collins, CO

[7]National Center for Atmospheric Research, Boulder, CO

Abstract

Space-borne observations of CO_2 from the Orbiting Carbon Observatory-2 are used to characterize the response of the tropical atmospheric CO_2 concentrations to the strong El Niño event of 2015–2016. Correlations between atmospheric CO_2 growth rate and the El Niño Southern Oscillation have been well known; however, the magnitude of the correlation and the timing of the responses of oceanic and terrestrial carbon cycle remain poorly constrained in space and time. Here we use space-based CO_2 observations to confirm that the tropical Pacific Ocean does play an early and important role in modulating the changes in atmospheric CO_2 concentrations during El Niño events – phenomenon inferred but not previously observed due to lack of high-density, broad-scale CO_2 observations over the Tropics.

El Niño Southern Oscillation, or ENSO, is the dominant mode of tropical climate variability on interannual to decadal timescales (1–5) and is correlated with large inter-annual variability in global atmospheric CO_2 concentrations (6–19). Studying the response of the carbon cycle to this natural climate phenomenon is critical to understand and quantify the sensitivity of the carbon cycle to climate variability, and by extension to climate generally (20). Although the ENSO cycle originates in the equatorial Pacific, its impact on the carbon cycle is felt globally due to its regional teleconnections (22–23) and influences on atmospheric and ocean circulation, precipitation, temperature, and fire emissions (1, 24–26). Partitioning the response of the constituent components of the carbon cycle to a complete El Niño event has been challenging because of the limited number of CO_2 observations over the tropical land and ocean regions.

*Correspondence to: abhishek.chatterjee@nasa.gov.

Observations of atmospheric CO_2 from space provide a global view of the carbon cycle that can be used to describe phenomena that have been previously pieced together from sparse *in situ* data. NASA's Orbiting Carbon Observatory-2 (OCO-2) mission was successfully launched on July 2, 2014 and started providing science data in early September 2014 (70). Within the first two years of operation of the OCO-2 mission, a major El Niño (warm phase of the ENSO) occurred (27–30). We provide an approach for studying the temporal sequence of El Niño-induced changes in global CO_2 concentrations using observations from the OCO-2 mission that are validated with the Tropical Atmosphere Ocean (TAO) mooring CO_2 data. We see a response from the tropical Pacific Ocean during the early stages of an El Niño event and a lagged (and much larger) terrestrial signal as the El Niño reaches maturity.

El Niño and the global carbon cycle

Correlations between the atmospheric CO_2 growth rate and El Niño activity have been reported since the 1970s (6–8, 31–32), although the magnitude and timing of the responses of the ocean and terrestrial components remain poorly constrained (33). Here, the word terrestrial includes both changes in biospheric productivity (respiration and photosynthesis) as well as biomass burning (fires). Following previous strong El Niño events (for example, the 1982–1983 and 1997–1998 El Niño events), methods for measuring the atmospheric CO_2 response to ENSO were based on *in situ* atmospheric CO_2 observations at a handful of surface stations that transect the tropical Pacific, including Mauna Loa, Christmas Island and American Samoa (8, 34) as well as shipboard transect measurements (12, 35–36). The annual growth rate of atmospheric CO_2 measured at these remote stations and other sites around the globe show remarkable correlation with ENSO indices, with a rapid increase in atmospheric CO_2 associated with the late stage of an El Niño event (19, 37). The ocean response to El Niño events is based on studies looking at *in situ* observations, for example, surface ocean pCO_2 observations from ships of opportunity (12), moorings (38–39), or targeted field campaigns during El Niño events (9–10, 40–41), and a variety of mechanistic ocean models (24, 52, 54, 61, 65, 67).

The overall increase in the release of CO_2 to the atmosphere during strong El Niño events has been attributed to a decrease in biospheric uptake of CO_2 (e.g., due to drying of tropical land regions and an increase in plant and soil respiration) combined with enhanced fire emissions. In recent years, this has led to a growing body of literature (42–49) concluding that ENSO-mediated variability in tropical net land primary productivity is what primarily influences the atmospheric CO_2 growth rate. A handful of studies (25, 50–51) have disputed any consistent or coherent response from the land component during El Niño events, thus highlighting the high level of uncertainty and disagreement within the carbon cycle community.

The El Niño-CO_2 signature should have a significant tropical Pacific Ocean component as well, with opposite sign to the terrestrial response (10, 13, 33). During strong El Niño events, there is a large-scale weakening of the easterly trade winds and suppression of eastern equatorial Pacific upwelling (indicated by a deeper thermocline) that reduces the supply of cold, carbon-rich waters to the surface (Fig. 1). This reduces the usual strong outgassing of CO_2 from this region (52–67), typically on the order of ~0.4–0.6 PgC yr^{-1} to

the atmosphere, by ~40–60% during an El Niño event (9–12, 33, 36, 60, 73). If net fluxes were to remain constant elsewhere, these substantial net air-sea CO_2 anomalies should lead to a reduction in the growth rate of atmospheric CO_2, at least during the early stages of El Niño.

Understanding these variations in atmospheric CO_2, the timing of these variations and the underlying processes that cause them have been of great interest within the carbon cycle community (1, 10–13, 15, 20, 33, 50). Integrating information from ocean- and atmosphere-based estimates, and modeling studies, we now know that it is the combined and opposite effect of ocean and terrestrial responses, which contribute to El Niño-related variations in atmospheric CO_2 (33). What remain controversial though are the timing of the ocean response and a precise quantification of its role. This is of crucial importance because typically the interannual variability (IAV) in the growth rate of atmospheric CO_2 is used to constrain the climate sensitivity of land carbon fluxes (γ_{LT}) (20–21); however, if a component of the IAV is being modified by ocean fluxes, then these inferences of γ_{LT} need to be reconsidered.

Because of the few surface CO_2 monitoring stations over the center of action (i.e., tropical Pacific Ocean), it has been challenging to directly observe the timing and changes in flux of CO_2 from the ocean to the atmosphere that affect the atmospheric CO_2 growth rate during an El Niño event. Efforts to analyze the data from distant measurement locations tend to identify the enhanced CO_2 fluxes from the terrestrial carbon cycle, which dominate during the later stages of El Niño. The high-density, broad-scale observations of CO_2 from OCO-2 provide a valuable tool to partition the ocean and terrestrial carbon cycle responses to El Niño.

Time series of X_{CO2} anomalies during the 2015–2016 El Niño

OCO-2 observations describe the column-averaged CO_2 dry air mole fraction (X_{CO2}). More details regarding the OCO-2 mission, data features, X_{CO2} retrievals, etc. are provided in the Supplementary Materials, and are available in (69) and (70) while validation of X_{CO2} via comparisons to a ground-based network are provided in (71).

El Niño events are identified by warm sea surface temperature anomalies in precise regions of the tropical Pacific Ocean, with the most commonly used being the Niño 3.4 region (5°S–5°N, 170°W–120°W). Figs. 2A and 2B show the trend in X_{CO2} anomaly (90) for the Niño 3.4 region and its temporal evolution relative to two ENSO indices (97), including the Oceanic Niño Index (ONI - derived from sea surface temperature anomalies in the Niño 3.4 region) and the Southern Oscillation Index (SOI - derived from observed sea level pressure differences between Tahiti and Darwin, Australia). The 2015–2016 El Niño began around March 2015 and reached its peak over the Central Pacific between November 2015 and January 2016 (30). The X_{CO2} anomaly (Fig. 2B) shows two distinct periods over the entire El Niño event: (a) Development phase of El Niño (Spring-Summer 2015) – we argue that the negative X_{CO2} anomaly is due to a reduction in local CO_2 outgassing from the tropical Pacific Ocean, and (b) Mature phase of El Niño (Fall 2015 onwards) – we argue that the positive trend in X_{CO2} anomaly reflects an increase in atmospheric CO_2 concentrations due

to terrestrial sources (i.e., combination of reduced vegetation uptake across pan-tropical regions and enhanced biomass burning emissions from SE Asia and Indonesia). The time series in Fig. 2B shows the space-based CO_2 dataset documenting the response of the carbon cycle (both oceanic and terrestrial) during an entire El Niño event, capturing both the development and the mature phase and the transition between those two. The timing of the OCO-2 launch was extremely fortuitous in this regard.

Deriving the X_{CO2} anomalies require observations taken by both NASA's OCO-2 and the Japan Aerospace Exploration Agency's (JAXA) Greenhouse Gases Observing Satellite (GOSAT) (68) mission. The short OCO-2 record makes it impossible to fit a long-time series and calculate anomalies, and hence data from the GOSAT mission (operating since January 2009) was utilized to generate the X_{CO2} climatology. The OCO-2 team retrieved X_{CO2} from the first 7 years of the GOSAT observations using the same retrieval algorithm that generated the OCO-2 data product (90). Continuous global coverage from these two missions allows us to stitch together a long-time series of X_{CO2} over remote regions, such as the tropical Pacific Ocean (Figs. S1–S2). However, utilizing two data sources, i.e., GOSAT and OCO-2, can incur errors in the analyses due to changes in the two instruments, their observing strategies and sampling density. Fig. 2B also illustrates the corresponding uncertainty in our analyses. The uncertainty is calculated using an ensemble technique (Section C in Supplementary Materials) and further brings out the two phases in the time series of the Niño 3.4 X_{CO2} anomaly – ±0.3 ppm uncertainties during the El Niño development phase with both the upper and lower bounds below the zero line, and larger uncertainties of ±0.5 ppm during the mature phase of the El Niño event. These larger uncertainties during the latter stages of the El Niño illustrate the challenge in attributing the changes in X_{CO2} anomalies to the competing, and often opposing, signals from the ocean and the terrestrial components of the carbon cycle.

Attributing the two observed phases of X_{CO2} anomalies to the ocean and the terrestrial response

Our argument for the two observed phases in the X_{CO2} anomaly time series is supported by complementary data sources. The ocean response is corroborated by sea surface pCO_2 observations from an *in situ* network of autonomous CO_2 systems on the TAO moored buoy array (9, 38, 72). Data are not directly comparable to atmospheric X_{CO2} as they describe CO_2 variations at the ocean surface. The trend of the difference between the sea surface and atmospheric CO_2 (ΔpCO_2), however, does capture typical El Niño signatures. For example, Fig. 2C illustrates data from one of the moored buoys in the Niño 3.4 region (0°, 170°W), which shows decreasing ΔpCO_2 over the spring and near-zero ΔpCO_2 by December 2015. A suppression in the upwelling of CO_2-rich waters caused by weakening of the easterly trade winds leads to a reduction in the surface ocean carbon content, which in turn leads to a decline in the magnitude of sea-to-air CO_2 fluxes. The flux estimates at this buoy location are 1.35 ± 0.21 (1σ) gC m^{-2} $month^{-1}$ during the November 2014 to February 2015 period (i.e., non El Niño conditions) that gradually decrease to 0.087 ± 0.083 (1σ) gC m^{-2} $month^{-1}$ between November 2015 and February 2016 (i.e., El Niño conditions). This indicates a near-total shutdown of sea- to-air flux during Boreal Winter 2015–2016 relative to the neutral

2014–2015 Boreal Winter. Previous studies focusing on the tropical Pacific Ocean have reported flux reductions of ~40– 60% over the entire basin (9–12, 33, 36, 60, 73). Atmospheric transport model calculations with a prescribed set of flux patterns and comparing to the observed X_{CO2} anomalies (Section A in Supplementary Materials) suggest a flux reduction of ~26–54%.

While these numbers are roughly similar, we do recognize the limitation in comparing flux estimates from one point (namely the TAO location at 0°, 170°W) to flux estimates for the entire Niño 3.4 region and/or the tropical Pacific Ocean from previous studies. Large-scale changes in the physical and biogeochemical dynamics during El Niño events result in significant spatial and temporal variability in the surface pCO_2 distributions (12, 62, 65). Additionally, these spatial variations and their seasonal progression are uniquely tied to each El Niño event; thus, different flavors of El Niño events and/or shifts in the El Niño phenomena (86–88) will influence the evolution of the seasonal cycle of pCO_2 and air-sea CO_2 fluxes over the region. For the 20152016 El Niño event, the TAO buoy at 0°, 170°W lay closest to the edge of the warm pool and registered the first response to the onset of El Niño conditions. As observations from other TAO locations (92) are becoming available, it is evident that in the eastern part of the basin there was an overall suppression of the outgassing CO_2 source but with large variability in pCO_2. Data synthesis and modeling work with these and other *in situ* observations are ongoing to quantify the exact magnitude of ocean CO_2 fluxes over different tropical Pacific regions during the 2015– 2016 El Niño.

The second phase in the X_{CO2} anomaly time series is driven by the terrestrial component of the carbon cycle, and the transport of this signal to the remote Niño 3.4 region. The anomalous increase in CO_2 can be attributed to a combination of terrestrial sources, including a reduction in the global biospheric uptake, increases in soil and plant respiration and enhanced fire emissions. In fact, the impact of enhanced fire emissions and their regional progression was a well-studied feature following the strong 1997–1998 El Niño (26, 43, 74–76). For the 2015–2016 El Niño event, strong correspondences between X_{CO2} from OCO-2 and the carbon monoxide (CO) total column anomalies from the Measurements of Pollution in the Troposphere (MOPITT) instrument on the NASA Terra platform, are evident over the tropical Pacific Ocean, especially during Fall 2015 (Fig. 2D). We conjecture that these CO total column anomalies are representative of the emissions from the 2015–2016 Indonesian peat fires (77–80), which were advected into the tropical Pacific region. El Niño-related changes in the Walker circulation (i.e., westerly winds) and the slightly more southern than normal positioning of the Inter Tropical Convergence Zone (ITCZ) (81) may allow emissions from the Indonesian peat fires to carry over into this region (Fig. S4). It is interesting to note from Figs. 2B and 2D that the positive increase in X_{CO2} anomaly actually leads the fire signals by 1–2 months. This indicates that the release of carbon flux resulting in an increase in CO_2 concentrations is only partially pyrogenic; reduced vegetation uptake due to droughts is a significant contributor, and quite possibly the initial cause of the increase in X_{CO2} anomaly.

Isolating the observed negative X_{CO2} anomaly to an ocean signal

The time dependence of the X_{CO2} anomalies during the 2015–2016 El Niño indicate that the initial decrease in atmospheric CO_2 is due to suppression of upwelling in the tropical Pacific. This early negative response is subsequently offset by a large positive anomaly due to the terrestrial component. Assuming no significant interannual changes elsewhere in the global ocean, we can further confirm our argument by a comparison of the X_{CO2} anomaly in the Niño 3.4 region with the global X_{CO2} anomaly (Fig. 4A). By differencing the far-field effect from the local signal, the influence of the reduction in CO_2 outgassing from the tropical Pacific Ocean is clearly visible during the onset phase of El Niño. The peak reduction registered over the Niño 3.4 region relative to the global X_{CO2} anomalies is 0.35 ppm in June 2015, which occurs a couple of months after the initiation of the El Niño event. Lag correlation of the Niño 3.4 X_{CO2} anomalies against the ONI index indicate that the highest positive correlation occurs when the concentration-related anomalies lag the SST-related anomalies by 1–2 months (93) (Fig. S8). The time lag relationship can be precisely quantified during the onset phase of El Niño, but it is much more difficult to interpret during the succeeding El Niño stages when any reduction in CO_2 from decreased equatorial upwelling is masked by the signal from terrestrial processes. Thus, if it were not for the reduction in outgassing from the ocean, the impact from the terrestrial sources would likely be larger. Our analysis confirms the findings from (13) that the slowdown of atmospheric CO_2 increase during the early stages of an El Niño is indeed related to the decreased sea-to-air flux of CO_2 in the tropical Pacific Ocean. The coverage from the OCO-2 mission has enabled us to verify this hypothesis and monitor its temporal evolution using real atmospheric CO_2 observations.

The early stage negative X_{CO2} anomaly is unique to the tropical Pacific Ocean and is not influenced by global, terrestrial or large-spatial scale fluxes. Due to the large interhemispheric gradients in CO_2, typical variability in tropical CO_2 concentrations can be an aliasing of terrestrial processes occurring at higher latitudes. In order to confirm that the recovered ocean signal in the X_{CO2} anomaly is unique to the tropical Pacific Ocean, we examined three other ocean regions - the subtropical North Pacific (20°–30°N, 120°–170°W), the subtropical South Pacific (20°–30°S, 120°–170°W) and the tropical Atlantic Ocean (5°N–5°S, 5°–35°W). Fig. 3 shows the specific regions (aside from Niño 3.4) that we have analyzed, and each of which assist us to reject alternative hypotheses. Non-zero differences in X_{CO2} anomalies between these and the Niño 3.4 region (Fig. 4) indicate that the trend observed over the tropical Pacific Ocean is distinct from other ocean basins. This makes intuitive sense from our mechanistic understanding as well - while large impacts of ENSO on the sea-to-air CO_2 flux in the tropical Pacific Ocean are expected, studies have shown minute and delayed influence of the ENSO modes on the variability of carbon fields in the tropical Atlantic Ocean (66, 82–83).

Perspective

The strong El Niño in 2015–2016 caused a reduction in the magnitude of CO_2 outgassing from the tropical Pacific Ocean. These changes, albeit of varying magnitude, extended over a large portion of the tropical Pacific, and impacted the large-scale modulation of the

physical processes responsible for the CO_2 efflux from this region. Almost all observing networks (i.e., OCO-2, TAO, etc.) were aided by the strength of this signal. However, OCO-2 provided a more comprehensive view of the tropical Pacific Ocean signal than previous observing networks given its: (a) greater coverage and more frequent sampling than *in situ* networks, and (b) improved resolution and precision than earlier space-based instruments. For example, GOSAT, like OCO-2 is sensitive to the total CO_2 column, but has lower precision (2 ppm single sounding random error for GOSAT vs. 0.5 ppm for OCO-2) and lower sampling density (100× less soundings). The immediate next step will be to fold in these observations into an inverse modeling framework (13, 15, 50, 56) to infer the underlying net fluxes between the ocean and atmosphere and the terrestrial biosphere and the atmosphere. This would help establish the real benefit of OCO-2, especially against the backdrop of previous studies that had to rely on sparse atmospheric constraint to infer changes in CO_2 surface fluxes during El Niño events.

Based on OCO-2 data alone, however, we cannot quantitatively discriminate the relative roles of reduction in biospheric activity uptake due to a warmer and drier climate in 2015 versus enhanced fire emissions. While we can quantify the temporal response of the ocean versus the terrestrial component and qualitatively observe the gradients in the response of different tropical Pacific Ocean regions (Fig. 5), it is much more challenging to discriminate the contribution of fire emissions and the delayed response of the terrestrial biosphere to El Niño-induced changes in weather patterns. The impact of ENSO is typically felt by the terrestrial biosphere over several months to a year after the actual event. Studies on both progressions of droughts (84) and fires (26) during an El Niño cycle have shown a hysteresis in the Earth system's response to changes in temperature and precipitation patterns. Analyses using ancillary data sources such as solar- induced fluorescence (SIF), bottom-up model simulations and inverse modeling calculations are typically necessary to quantify the partitioning of the terrestrial carbon fluxes (reduction in biospheric uptake vs. increase in fire emissions) as has been pursued in a companion study (85).

Our study provides a short-term perspective on the potential of CO_2 observations from space for unraveling more complex relationships of carbon sources and sinks in the future. A longer time series of observations will enable testing more hypotheses such as the possibility of regionally dependent gradients in air-sea CO_2 fluxes in the tropical Pacific, or adding data to support biogeochemical theories at previously inaccessible scales. From a long-term perspective, such information will improve our process-based understanding, inform our current suite of mechanistic models, and ultimately, better constrain future carbon cycle projections.

Concluding remarks

The strong El Niño event of 2015–2016 provided us with an opportunity to study how the global carbon cycle responds to changes in the physical climate system. With the high-resolution (both spatial and temporal) observations available from OCO-2, we are able to directly: (a) observe the strong correlations that exist between atmospheric CO_2 concentrations and the El Niño signal, and (b) track the development of the atmospheric CO_2 anomaly as it switches from a negative phase (i.e., due to a reduction in CO_2 outgassing

from the tropical Pacific Ocean) to a strong positive phase (i.e., due to a reduction in biospheric uptake and increased fire emissions). The most important contribution of the space-based OCO-2 mission is the ability to observe and monitor carbon cycle phenomena at high-density over large spatial scales, which has not been possible from the existing *in situ* network.

The complexity of the El Niño – CO_2 signature illustrates that it is a multifaceted system with contributions from many regions and processes. Understanding and predicting its behavior requires separating out the many terrestrial and marine regions that contribute (1, 33) and identifying both the geophysical (3, 27, 30) and the biological (10, 59, 89) phenomena that respond in their own unique ways. However, the impact on the carbon cycle is unified through the global mixing of CO_2 in the atmosphere - OCO-2 makes a unique contribution by providing both the global coverage and fine surface spatial detail; alongside the *in situ* CO_2 network of moorings and shipboard measurements provide the long-term climate-quality record of atmospheric and ocean CO_2 observations and serves to validate the OCO-2 observations and model products. We emphasize that this diverse observing portfolio is necessary, and the complementary information provided by these observing systems will likely prove critical in understanding the partitioning of carbon fluxes during the 2015–2016 El Niño, the relative contribution of ocean vs. land to the global atmospheric CO_2 growth rate, and the sensitivity of the carbon cycle to climate forcing on interannual to decadal timescales.

Supplementary Material

Refer to Web version on PubMed Central for supplementary material.

Acknowledgments

This work was supported by funding from the NASA ROSES-2014 Grant/Cooperative Agreement Number NNX15AG92G. A portion of this research was carried out at the Jet Propulsion Laboratory, California Institute of Technology, under a contract with the National Aeronautics and Space Administration. The work of B.B.S was supported by NCAR, which is sponsored by the National Science Foundation. The work of A.J.S. and R.A.F. was funded by the Office of Oceanic and Atmospheric Research (OAR) of the National Oceanic and Atmospheric Administration (NOAA), U.S. Department of Commerce, including resources from the Ocean Observation and Monitoring Division (OOMD) of the Climate Program Office (FundRef number 100007298). This is Pacific Marine Environmental Laboratory Contribution No. 4607.

The OCO-2 and GOSAT-ACOS data were produced by the ACOS/OCO-2 project at the Jet Propulsion Laboratory, California Institute of Technology, and obtained from the free ACOS/OCO-2 data archive maintained at the NASA Goddard Earth Science Data and Information Services Center (https://disc.gsfc.nasa.gov/OCO-2). The MOPITT datasets were obtained from the NASA Langley Research Center Atmospheric Science Data Center (https://eosweb.larc.nasa.gov/project/mopitt/mopitt_table). The authors gratefully acknowledge the National Data Buoy Center for supporting deployment and recovery of the moored pCO_2 systems and maintenance of the TAO buoys.

Finally, the authors would like to acknowledge the comments from the editor and three anonymous reviewers, discussions with Helen Worden (NCAR), John Worden (JPL), Paul Wennberg (Caltech), Steven Pawson (NASA), Stephen Cohn (NASA), Lesley Ott (NASA) and Brad Weir (USRA), and graphic design help from David Hinkle (JPL) and Sterling Spangler (SSAI).

References and Notes

1. McPhaden MJ, Zebiak SE, Glantz MH. ENSO as an integrating concept in Earth science. Science. 2006; 314:1740–1745. [PubMed: 17170296]

2. Philander, SG. El Niño, La Niña, and the Southern Oscillation. Academic Press; San Diego, CA: 1990.
3. Neelin JD, et al. ENSO theory. Journal of Geophysical Research-Oceans. 1998; 103:14261–14290.
4. Trenberth KE. The definition of El Niño. Bulletin of the American Meteorological Society. 1997; 78:2771–2777.
5. Cane MA. The evolution of El Niño, past and future. Earth and Planetary Science Letters. 2005; 230:227–240.
6. Bacastow RB, et al. Atmospheric carbon-dioxide, the southern oscillation, and the weak 1975 El-Niño. Science. 1980; 210:66–68. [PubMed: 17751153]
7. Keeling CD, Revelle R. Effects of El-Niño Southern Oscillation on the atmospheric content of carbon dioxide. Meteoritics. 1985; 20:437–450.
8. Keeling CD, et al. Interannual extremes in the rate of rise of atmospheric carbon dioxide since 1980. Nature. 1995; 375:666–670.
9. Chavez FP, et al. Biological and chemical response of the equatorial Pacific Ocean to the 1997–98 El Niño. Science. 1999; 286:2126–2131. [PubMed: 10591638]
10. Feely RA, et al. Influence of El Niño on the equatorial Pacific contribution to atmospheric CO_2 accumulation. Nature. 1999; 398:597–601.
11. Feely RA, et al. Seasonal and interannual variability of CO_2 in the equatorial Pacific. Deep-Sea Research Part II-Topical Studies in Oceanography. 2002; 49:2443–2469.
12. Feely RA, et al. Decadal variability of the air-sea CO_2 fluxes in the equatorial Pacific Ocean. Journal of Geophysical Research-Oceans. 2006; 111:16.
13. Rayner PJ, Law RM, Dargaville R. The relationship between tropical CO_2 fluxes and the El Niño-Southern Oscillation. Geophysical Research Letters. 1999; 26:493–496.
14. Jones CD, et al. The carbon cycle response to ENSO: A coupled climate-carbon cycle model study. Journal of Climate. 2001; 14:4113–4129.
15. Peylin P, et al. Multiple constraints on regional CO_2 flux variations over land and oceans. GlobalBiogeochemical Cycles. 2005; 19:21.
16. Gurney KR, et al. Interannual variations in continental-scale net carbon exchange and sensitivity to observing networks estimated from atmospheric CO_2 inversions for the period 1980 to 2005. Global Biogeochemical Cycles. 2008; 22:17.
17. Nevison CD, et al. Contribution of ocean, fossil fuel, land biosphere, and biomass burning carbon fluxes to seasonal and interannual variability in atmospheric CO_2. Journal of Geophysical Research-Biogeosciences. 2008; 113:21.
18. Jiang X, et al. Interannual variability of mid-tropospheric CO_2 from Atmospheric Infrared Sounder. Geophysical Research Letters. 2010; 37:5.
19. Betts R, et al. El Niño and a record CO_2 rise. Nature Climate Change. 2016; 6:806–810.
20. Cox PM, et al. Sensitivity of tropical carbon to climate change constrained by carbon dioxide variability. Nature. 2013; 494:341–344. [PubMed: 23389447]
21. Wenzel S, et al. Emergent constraints on climate-carbon cycle feedbacks in the CMIP5 Earth system models. Journal of Geophysical Research-Biogeosciences. 2014; 119:794–807.
22. Trenberth KE, et al. Progress during TOGA in understanding and modeling global teleconnections associated with tropical sea surface temperatures. Journal of Geophysical Research-Oceans. 1998; 103:14291–14324.
23. Tribbia, JJ. The rudimentary theory of atmospheric teleconnections associated with ENSO. In: Glantz, MH.Katz, RW., Nicholls, N., editors. Teleconnections Linking Worldwide Climate Anomalies. Cambridge University Press; New York: 1991. p. 285-308.
24. Resplandy L, Séférian R, Bopp L. Natural variability of CO_2 and O_2 fluxes: What can we learn from centuries-long climate models simulations? Journal of Geophysical Research-Oceans. 2015; 120:384–404.
25. Woodward FI, Lomas MR, Quaife T. Global responses of terrestrial productivity to contemporary climatic oscillations. Philosophical Transactions of the Royal Society B-Biological Sciences. 2008; 363:2779–2785.

26. Le Page Y, et al. Global fire activity patterns (1996–2006) and climatic influence: an analysis using the World Fire Atlas. Atmospheric Chemistry and Physics. 2008; 8:1911–1924.
27. McPhaden MJ. COMMENTARY: Playing hide and seek with El Niño. Nature Climate Change. 2015; 5:791–795.
28. Levine AFZ, McPhaden MJ. How the July 2014 easterly wind burst gave the 2015– 2016 El Niño a head start. Geophysical Research Letters. 2016; 43:6503–6510.
29. Gasparin F, Roemmich D. The strong freshwater anomaly during the onset of the 2015/2016 El Niño. Geophysical Research Letters. 2016; 43:6452–6460.
30. Paek H, Yu J-Y, Qian C. Why were the 2015/2016 and 1997/1998 extreme El Niños different? Geophysical Research Letters. 2017; 44:1848–1856.
31. Bacastow RB. Modulation of atmospheric carbon dioxide by southern oscillation. Nature. 1976; 261:116–118.
32. Newell RE, Weare BC. A relationship between atmospheric carbon dioxide and Pacific sea surface temperatures. Geophysical Research Letters. 1977; 4:1–2.
33. Sarmiento, JL., Gruber, N. Ocean Biogeochemical Dynamics. Princeton University Press; Princeton, NJ: 2006. Carbon Cycle, CO_2 and Climate; p. 392-453.
34. Manning AC, et al. Interpreting the seasonal cycles of atmospheric oxygen and carbon dioxide concentrations at American Samoa Observatory. Geophysical Research Letters. 2003; 30:4.
35. Feely RA, et al. Effects of wind speed and gas exchange parameterizations on the air- sea CO_2 fluxes in the equatorial Pacific Ocean. Journal of Geophysical Research-Oceans. 2004; 109:10.
36. Ishii M, et al. Air-sea CO_2 flux in the Pacific Ocean for the period 1990–2009. Biogeosciences. 2014; 11:709–734.
37. Jones CD, Cox PM. On the significance of atmospheric CO_2 growth rate anomalies in 2002-2003. Geophysical Research Letters. 2005; 32:4.
38. Sutton AJ, et al. Natural variability and anthropogenic change in equatorial Pacific surface ocean pCO_2 and pH. Global Biogeochemical Cycles. 2014; 28:131–145.
39. Sutton AJ, et al. A high-frequency atmospheric and seawater pCO_2 data set from 14 open-ocean sites using a moored autonomous system. Earth System Science Data. 2014; 6:353–366.
40. Feely RA, et al. Distribution of chemical tracers in the eastern equatorial pacific during and after the 1982–1983 El Niño southern oscillation event. Journal of Geophysical Research-Oceans. 1987; 92:6545–6558.
41. Feely RA, et al. Variability of CO_2 distributions and sea-air fluxes in the central and eastern equatorial Pacific during the 1991–1994 El Niño. Deep-Sea Research Part II-Topical Studies in Oceanography. 1997; 44:1851–1867.
42. Hashimoto H, et al. El Niño-Southern Oscillation-induced variability in terrestrial carbon cycling. Journal of Geophysical Research-Atmospheres. 2004; 109:8.
43. Patra PK, et al. Role of biomass burning and climate anomalies for land-atmosphere carbon fluxes based on inverse modeling of atmospheric CO_2. Global Biogeochemical Cycles. 2005; 19:10.
44. van der Werf GR, et al. Interannual variability in global biomass burning emissions from 1997 to 2004. Atmospheric Chemistry and Physics. 2006; 6:3423–3441.
45. Qian H, Joseph R, Zeng N. Response of the terrestrial carbon cycle to the El Niño-Southern Oscillation. Tellus Series B-Chemical and Physical Meteorology. 2008; 60:537–550.
46. Li WH, et al. Impact of two different types of El Niño events on the Amazon climate and ecosystem productivity. Journal of Plant Ecology. 2011; 4:91–99.
47. Iguchi T. Correlations between interannual variations of simulated global and regional CO_2 fluxes from terrestrial ecosystems and El Niño Southern Oscillation. Tellus Series B-Chemical and Physical Meteorology. 2011; 63:196–204.
48. Wang WL, et al. Variations in atmospheric CO_2 growth rates coupled with tropical temperature. Proceedings of the National Academy of Sciences of the United States of America. 2013; 110:13061–13066. [PubMed: 23884654]
49. Anderegg WRL, et al. Tropical nighttime warming as a dominant driver of variability in the terrestrial carbon sink. Proceedings of the National Academy of Sciences of the United States of America. 2015; 112:15591–15596. [PubMed: 26644555]

50. Bousquet P, et al. Regional changes in carbon dioxide fluxes of land and oceans since 1980. Science. 2000; 290:1342–1346. [PubMed: 11082059]
51. Schwalm CR, et al. Does terrestrial drought explain global CO_2 flux anomalies induced by El Niño? Biogeosciences. 2011; 8:2493–2506.
52. Winguth AME, et al. El Niño Southern Oscillation related fluctuations of the marine carbon cycle. Global Biogeochemical Cycles. 1994; 8:39–63.
53. Feely RA, et al. CO_2 distributions in the equatorial Pacific during the 1991–1992 ENSO event. Deep-Sea Research Part II-Topical Studies in Oceanography. 1995; 42:365–386.
54. Le Quere C, et al. Interannual variability of the oceanic sink of CO_2 from 1979 through 1997. Global Biogeochemical Cycles. 2000; 14:1247–1265.
55. Behrenfeld MJ, et al. Biospheric primary production during an ENSO transition. Science. 2001; 291:2594–2597. [PubMed: 11283369]
56. McKinley GA, et al. Pacific dominance to global air-sea CO_2 flux variability: A novel atmospheric inversion agrees with ocean models. Geophysical Research Letters. 2004; 31:4.
57. Takahashi T, et al. Climatological mean and decadal change in surface ocean pCO_2, and net sea-air CO_2 flux over the global oceans. Deep-Sea Research Part II-Topical Studies in Oceanography. 2009; 56:554–577.
58. Park GH, et al. Variability of global net sea-air CO_2 fluxes over the last three decades using empirical relationships. Tellus Series B-Chemical and Physical Meteorology. 2010; 62:352–368.
59. Gierach MM, et al. Biological response to the 1997–98 and 2009–10 El Niño events in the equatorial Pacific Ocean. Geophysical Research Letters. 2012; 39:6.
60. Wanninkhof R, et al. Global ocean carbon uptake: magnitude, variability and trends. Biogeosciences. 2013; 10:1983–2000.
61. Long MC, et al. Twentieth-Century Oceanic Carbon Uptake and Storage in CESM1(BGC). Journal of Climate. 2013; 26:6775–6800.
62. Landschützer P, et al. Recent variability of the global ocean carbon sink. Global Biogeochemical Cycles. 2014; 28:927–949.
63. Landschützer P, Gruber N, Bakker DCE. Decadal variations and trends of the global ocean carbon sink. Global Biogeochemical Cycles. 2016; 30:1–22.
64. Rödenbeck C, et al. Interannual sea-air CO_2 flux variability from an observation-driven ocean mixed-layer scheme. Biogeosciences. 2014; 11:4599–4613.
65. Valsala VK, et al. Spatiotemporal characteristics of seasonal to multidecadal variability of pCO_2 and air-sea CO_2 fluxes in the equatorial Pacific Ocean. Journal of Geophysical Research-Oceans. 2014; 119:8987–9012.
66. Wang XJ, et al. Seasonal to decadal variations of sea surface pCO_2 and sea-air CO_2 flux in the equatorial oceans over 1984–2013: A basin-scale comparison of the Pacific and Atlantic Oceans. Global Biogeochemical Cycles. 2015; 29:597–609.
67. Obata A, Kitamura Y. Interannual variability of the sea-air exchange of CO_2 from 1961 to 1998 simulated with a global ocean circulation-biogeochemistry model. Journal of Geophysical Research. 2003; 108:3337.
68. Kuze A, et al. Thermal and near infrared sensor for carbon observation Fourier-transform spectrometer on the Greenhouse Gases Observing Satellite for greenhouse gases monitoring. Applied Optics. 2009; 48:6716–6733. [PubMed: 20011012]
69. Crisp D, et al. The on-orbit performance of the Orbiting Carbon Observatory-2 (OCO-2) instrument and its radiometrically calibrated products. Atmospheric Measurement Techniques. 2017; 10:59–81.
70. Eldering AE, et al. The Orbiting Carbon Observatory-2: first 18 months of science data products. Atmospheric Measurement Techniques. 2017; 10:549–563.
71. Wunch D, et al. Comparisons of the Orbiting Carbon Observatory-2 (OCO-2) X_{CO2} measurements with TCCON. Atmospheric Measurement Techniques. 2017; 10:2209–2238.
72. McPhaden MJ, et al. The tropical ocean global atmosphere observing system: A decade of progress. Journal of Geophysical Research-Oceans. 1998; 103:14169–14240.

73. Takahashi T, et al. Decadal variation of the surface water pCO_2 in the western and central equatorial Pacific. Science. 2003; 302:852–856. [PubMed: 14593175]
74. Page SE, et al. The amount of carbon released from peat and forest fires in Indonesia during 1997. Nature. 2002; 420:61–65. [PubMed: 12422213]
75. Langenfelds RL, et al. Interannual growth rate variations of atmospheric CO_2 and its delta C-13, H-2, CH_4, and CO between 1992 and 1999 linked to biomass burning. Global Biogeochemical Cycles. 2002; 16:1048–1069.
76. van der Werf GR, et al. Continental-scale partitioning of fire emissions during the 1997 to 2001 El Niño/La Nina period. Science. 2004; 303:73–76. [PubMed: 14704424]
77. Parker RJ, et al. Atmospheric CH_4 and CO_2 enhancements and biomass burning emission ratios derived from satellite observations of the 2015 Indonesian fire plumes. Atmospheric Chemistry and Physics. 2016; 16:10111–10131.
78. Huijnen V, et al. Fire carbon emissions over maritime southeast Asia in 2015 largest since 1997. Scientific Reports. 2016; 6:8. [PubMed: 28442703]
79. Field RD, et al. Indonesian fire activity and smoke pollution in 2015 show persistent nonlinear sensitivity to El Niño-induced drought. Proceedings of the National Academy of Sciences of the United States of America. 2016; 113:9204–9209. [PubMed: 27482096]
80. Yin Y, et al. Variability of fire carbon emissions in equatorial Asia and its nonlinear sensitivity to El Niño. Geophysical Research Letters. 2016; 43:10472–10479.
81. Schneider T, Bischoff T, Haug GH. Migrations and dynamics of the intertropical convergence zone. Nature. 2014; 513:45–53. [PubMed: 25186899]
82. McKinley GA, et al. Convergence of atmospheric and North Atlantic carbon dioxide trends on multidecadal timescales. Nature Geoscience. 2011; 4:606–610.
83. Lefèvre N, Caniaux G, Janicot S, Gueye AK. Increased CO_2 outgassing in February–May 2010 in the tropical Atlantic following the 2009 Pacific El Niño. Journal of Geophysical Research-Oceans. 2013; 118:1645–1657.
84. Vicente-Serrano SM, et al. A multiscalar global evaluation of the impact of ENSO on droughts. Journal of Geophysical Research-Atmospheres. 2011; 116:23.
85. Liu J, et al. Contrasting carbon cycle responses of the tropical continents to the 2015 El Niño. Science. **THIS ISSUE**, xx (xxxx).
86. Kug J-S, Jin FF, An S. Two types of El Niño events: cold tongue El Niño and warm pool El Niño. Journal of Climate. 2009; 22:1499–1515.
87. Ashok K, Yamagata T. The El Niño with a difference. Nature. 2009; 461:481–484. [PubMed: 19779440]
88. McPhaden MJ, Lee T, McClurg D. El Niño and its relationship to changing background conditions in the tropical Pacific Ocean. Geophysical Research Letters. 2011; 38:L15709.
89. Pala C. CLIMATE Corals tie stronger El Niños to climate change. Science. 2016; 354:1210. [PubMed: 27940821]
90. Procedure for generating the X_{CO2} climatology, calculating the anomaly, sensitivity tests to ascertain its robustness, and associated caveats are described in the Materials and Methods in the Supplementary Materials.
91. See the full list at - http://www.esrl.noaa.gov/psd/data/climateindices/list/
92. Data from other TAO locations (for example, at 0°, 110°W) demonstrate the heterogeneity in CO_2 concentrations as we move from west-to-east over the tropical Pacific Ocean. These data can be viewed at - http://www.pmel.noaa.gov/co2/story/OpenOceanMoorings
93. Bacastow (31) found the lag between one of the El Niño indices (SOI) and the CO_2 concentration changes to be 2.5 months at Mauna Loa and 6 months at South Pole. Rayner et al. (13) found in their study that CO_2 data anomalies lag the SOI by one month. Later Jones et al. (14) claimed that Mauna Loa CO_2 lagged behind Niño 3 SST anomalies by 3 months. The handful of studies illustrate the range of ENSO indices and atmospheric CO_2 dataset that have been employed; however, all of these studies were impacted by a lack of broad-scale observations over the tropical Pacific during the different phases of an El Niño event. This study provides a refinement of these earlier estimates of the time lags using higher-density space-based observations.

94. Crisp D, et al. The orbiting carbon observatory (OCO) mission. Trace Constituents in the Troposphere and Lower Stratosphere. 2004; 34:700–709.
95. Pollock R, et al. The Orbiting Carbon Observatory instrument: performance of the OCO instrument and plans for the OCO-2 instrument. Proc SPIE 7826, Sensors, Systems and Next Generation Satellites – XIV. 2010; 78260W
96. Taylor TE, et al. Orbiting Carbon Observatory-2 (OCO-2) cloud screening algorithms: validation against collocated MODIS and CALIOP data. Atmospheric Measurement Techniques. 2016; 9:973–989.
97. Nelson R, et al. The potential of clear-sky carbon dioxide satellite retrievals. Atmospheric Measurement Techniques. 2016; 9:1671–1684.
98. O'Dell C, et al. The ACOS CO_2 retrieval algorithm – Part 1: Description and validation against synthetic observations. Atmospheric Measurement Techniques. 2012; 5:99–121.
99. Crisp D, et al. The ACOS CO_2 retrieval algorithm–Part II: Global X_{CO2} data characterization. Atmospheric Measurement Techniques. 2012; 5:687–707.
100. Worden J, et al. Evaluation, Validation, And Attribution Of OCO-2 X_{CO2} Uncertainties. Atmos Meas Tech Disc. 2016 Available at. in review.
101. Lindqvist H, et al. Does GOSAT capture the true seasonal cycle of carbon dioxide? Atmospheric Chemistry and Physics. 2015; 15:13023–13040.
102. Schneising O, et al. Long-term analysis of carbon dioxide and methane column-averaged mole fractions retrieved from SCIAMACHY. Atmospheric Chemistry and Physics. 2011; 11:2863–2880.
103. Fortuin JPF, Kelder H. An ozone climatology based on ozonesonde and satellite measurements. Journal of Geophysical Research-Atmospheres. 1998; 103:31709–31734.
104. Randel WJ, Wu F. A stratospheric ozone profile data set for 1979–2005: Variability, trends, and comparisons with column ozone data. Journal of Geophysical Research-Atmospheres. 2007; 112:D06313.
105. McPeters RD, Labow GJ. Climatology 2011: An MLS and sonde derived ozone climatology for satellite retrieval algorithms. Journal of Geophysical Research- Atmospheres. 2012; 117:D10303.
106. Nguyen H, Cressie N, Braverman A. Multivariate Spatial Data Fusion for Very Large Remote Sensing Datasets. Remote Sensing. 2017; 9:142.
107. Weiss RF. Carbon dioxide in water and seawater: the solubility of a non-ideal gas. Marine Chemistry. 1974; 2:203–215.
108. Deeter MN, et al. Operational carbon monoxide retrieval algorithm and selected results for the MOPITT instrument. Journal of Geophysical Research-Atmospheres. 2003; 108:4399.
109. Emmons L, et al. Validation of Measurements of Pollution in the Troposphere (MOPITT) CO retrievals with aircraft in situ profiles. Journal of Geophysical Research-Atmospheres. 2004; 109:13.
110. Worden HM, et al. Decadal record of satellite carbon monoxide observations. Atmospheric Chemistry and Physics. 2013; 13:837–850.
111. Yin Y, et al. Decadal trends in global CO emissions as seen by MOPITT. Atmospheric Chemistry and Physics. 2015; 15:13433–13451.
112. Deeter MN, et al. The MOPITT Version 6 product: algorithm enhancements and validation. Atmospheric Measurement Techniques. 2014; 7:3623–3632.
113. Deeter MN, et al. Validation and analysis of MOPITT CO observations of the Amazon Basin. Atmospheric Measurement Techniques. 2016; 9:3999–4012.
114. Lamarque JF, et al. Identification of CO plumes from MOPITT data: Application to the August 2000 Idaho-Montana forest fires. Geophysical Research Letters. 2003; 30:1688.
115. Arellano A, et al. Time-dependent inversion estimates of global biomass-burning CO emissions using Measurement of Pollution in the Troposphere (MOPITT) measurements. Journal of Geophysical Research-Atmospheres. 2006; 111:D09303.
116. Jiang Z, et al. Impact of model errors in convective transport on CO source estimates inferred from MOPITT CO retrievals. Journal of Geophysical Research-Atmospheres. 2013; 118:2073–2083.

117. Worden J, et al. El Niño, the 2006 Indonesian peat fires, and the distribution of atmospheric methane. Geophysical Research Letters. 2013; 40:4938–4943.
118. Wanninkhof R. Relationship between the wind speed and gas exchange over the ocean revisited. Limnology and Oceanography - Methods. 2014; 12:351–362.
119. Bosilovich MG, et al. MERRA-2: File Specification. Tech Rep Global Modeling and Assimilation Office, Office Note No. 9. 2016
120. Gurney KR, et al. TransCom 3 CO_2 inversion intercomparison: 1. Annual mean control results and sensitivity to transport and prior flux information. Tellus Series B-Chemical and Physical Meteorology. 2003; 55:555–579.
121. Gurney KR, et al. Towards robust regional estimates of CO_2 sources and sinks using atmospheric transport models. Nature. 2002; 415:626–630. [PubMed: 11832942]
122. Pickers PA, Manning AC. Investigating bias in the application of curve fitting programs to atmospheric time series. Atmospheric Measurement Techniques. 2015; 8:1469–1489.
123. Thoning KW, Tans PP, Komhyr WD. Atmospheric carbon dioxide at Mauna Loa Observatory, 2. Analysis of the NOAA/GMCC data, 1974–1985. Journal of Geophysical Research-Atmospheres. 1989; 94:8549–8565.
124. Ebisuzaki W. A Method to Estimate the Statistical Significance of a Correlation When the Data Are Serially Correlated. Journal of Climate. 1997; 10:2147–2153.

One Sentence Summary

NASA's OCO-2 mission provides a first-hand look at the space-time evolution of tropical atmospheric CO_2 concentrations in response to the 2015–2016 El Niño

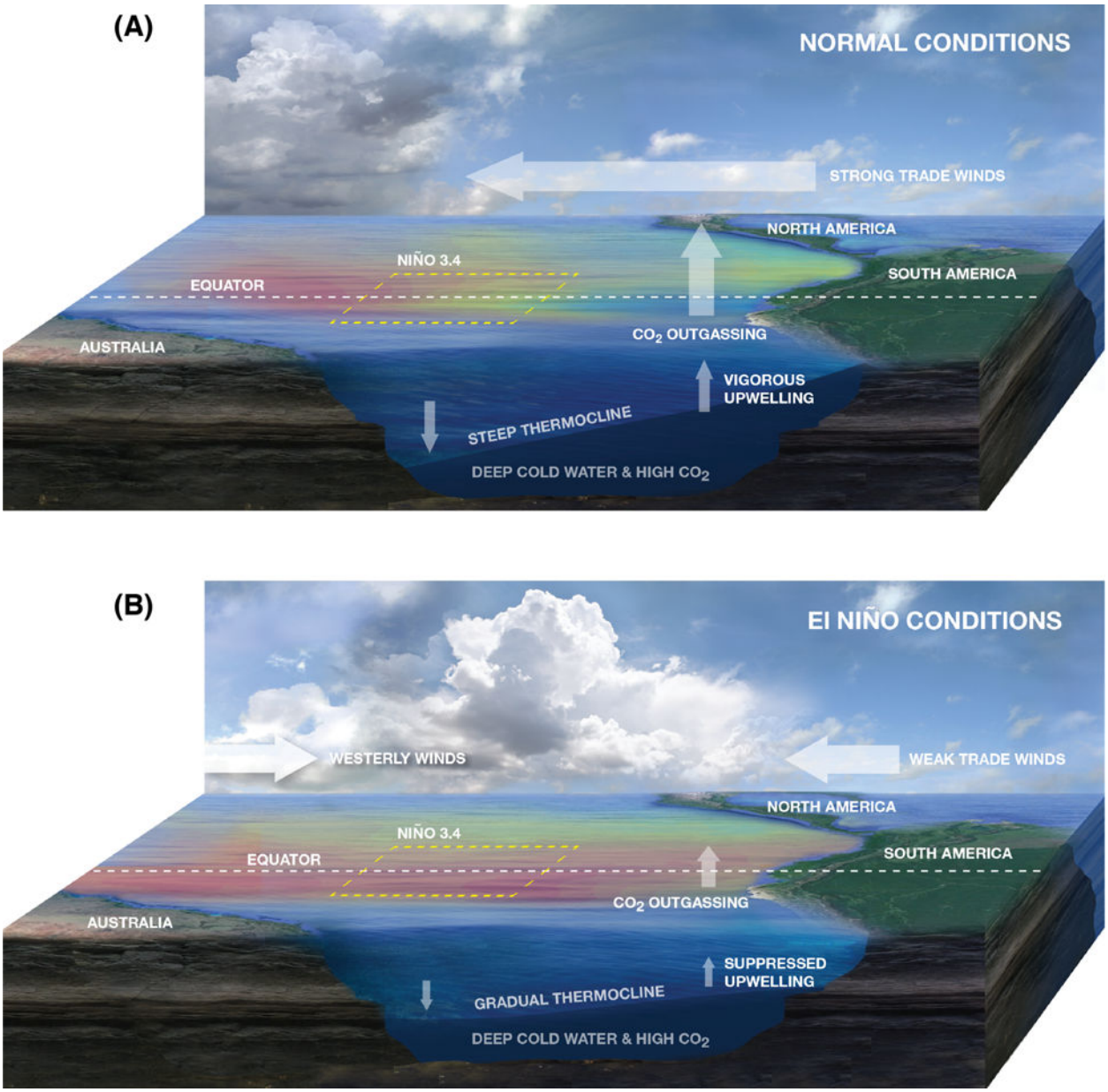

Fig. 1.

Schematic of the mechanistic differences between normal (A) and El Niño (B) conditions and associated carbon response over the tropical Pacific Ocean. Warm ocean surface temperatures are denoted in red and cooler waters in blue. During El Niño conditions, easterly trade winds weaken and westerly wind bursts occur. In association with the shift in wind regimes, the western tropical Pacific warm pool moves eastward and the slope of the thermocline flattens in the central and eastern tropical Pacific. This suppresses upwelling of cold, carbon-rich waters in the central and eastern tropical Pacific, reducing the magnitude of CO_2 outgassing into the atmosphere. Also shown are changes in atmospheric convection, wherein convection shifts eastward in response to eastward displacement of western tropical Pacific warm pool waters.

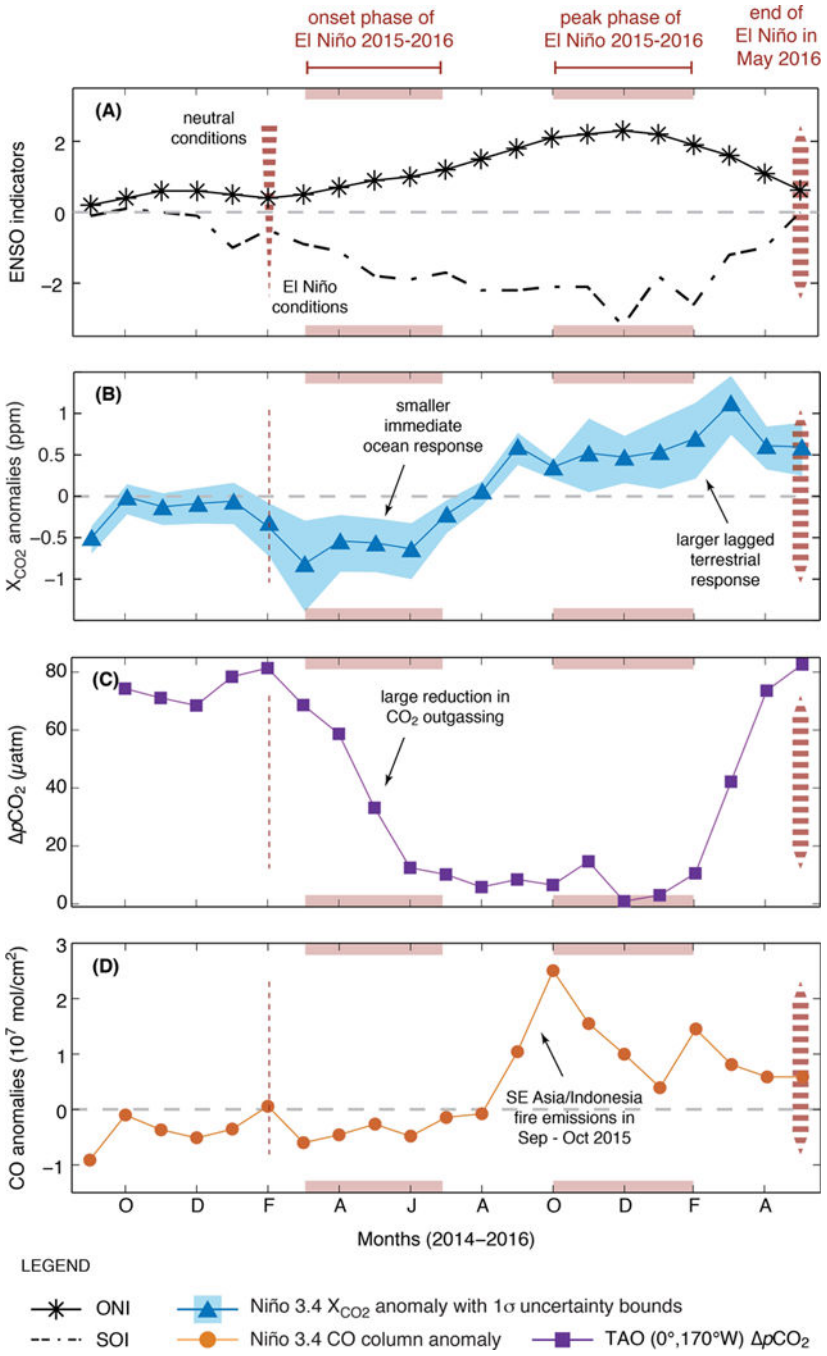

Fig. 2.

OCO-2 observes the response of the carbon cycle for an entire El Niño event. Temporal evolution of (A) the 2015–2016 El Niño as captured by the ONI and the SOI indices, (B) X_{CO2} anomalies and associated uncertainties in the Niño 3.4 region, (C) ΔpCO_2 from the TAO 0°, 170°W mooring, and (D) the CO total column anomalies in the Niño 3.4 region.

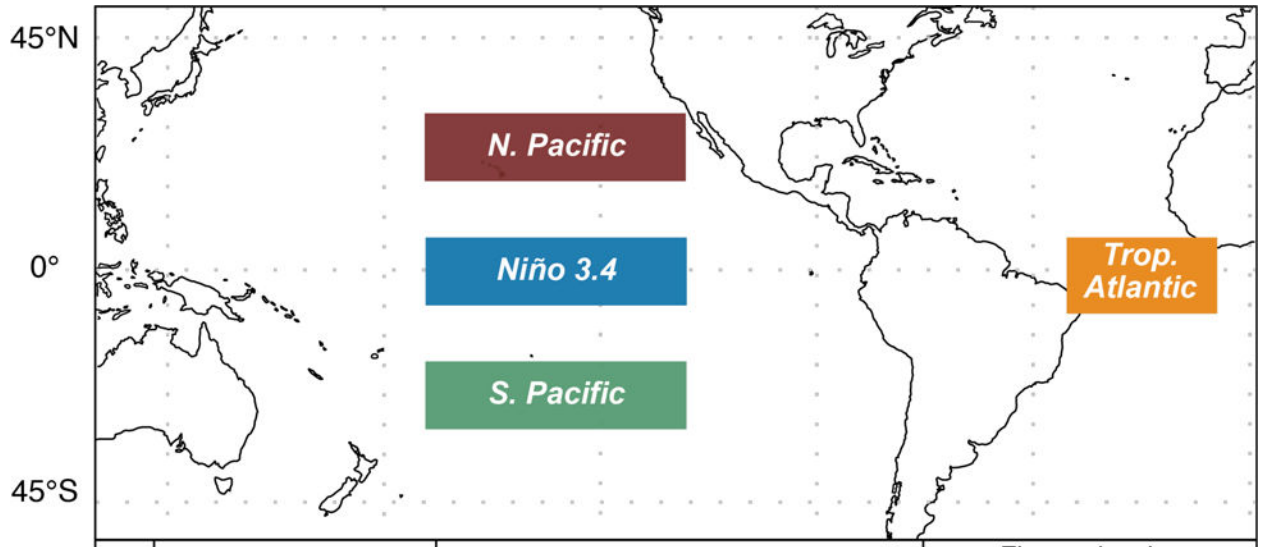

	Specific region analyzed	Alternative hypothesis	Figure showing difference between analyzed region and Niño 3.4
	Global (90°N -90°S, 0°-360°E)	X_{CO2} anomalies over the Pacific Ocean are responding to changes in terrestrial CO_2 concentrations	Fig. 4A
	Tropical Atlantic (5°N -5°S, 5°-35°W)	X_{CO2} anomalies over the Pacific Ocean are responding to changes in global CO_2 concentrations	Fig. 4B
	North Pacific (20°-30°N, 120°-170°W)	X_{CO2} anomalies over the tropical Pacific Ocean are responding to changes in CO_2 concentrations across the entire Pacific Ocean	Fig. 4C
	South Pacific (20°-30°S, 120°-170°W)	X_{CO2} anomalies over the tropical Pacific Ocean are responding to changes in CO_2 concentrations across the entire Pacific Ocean	Fig. 4C

Fig. 3.

Schematic showing the specific ocean basins (Niño 3.4, N. Pacific, S. Pacific and Trop. Atlantic) that were analyzed in this study. X_{CO2} anomalies are calculated for these different ocean basins, and subsequently compared to the X_{CO2} anomalies from the Niño 3.4 region. Each of these regions was considered to accept/reject a specific hypothesis that could potentially bias the observed trend in the Niño 3.4 X_{CO2} anomalies. After rejecting these hypotheses, we conclude that the negative X_{CO2} anomaly observed over the Niño 3.4 during the onset phase of El Niño 2015–2016 is unique and has to be driven by local changes in the ocean fluxes.

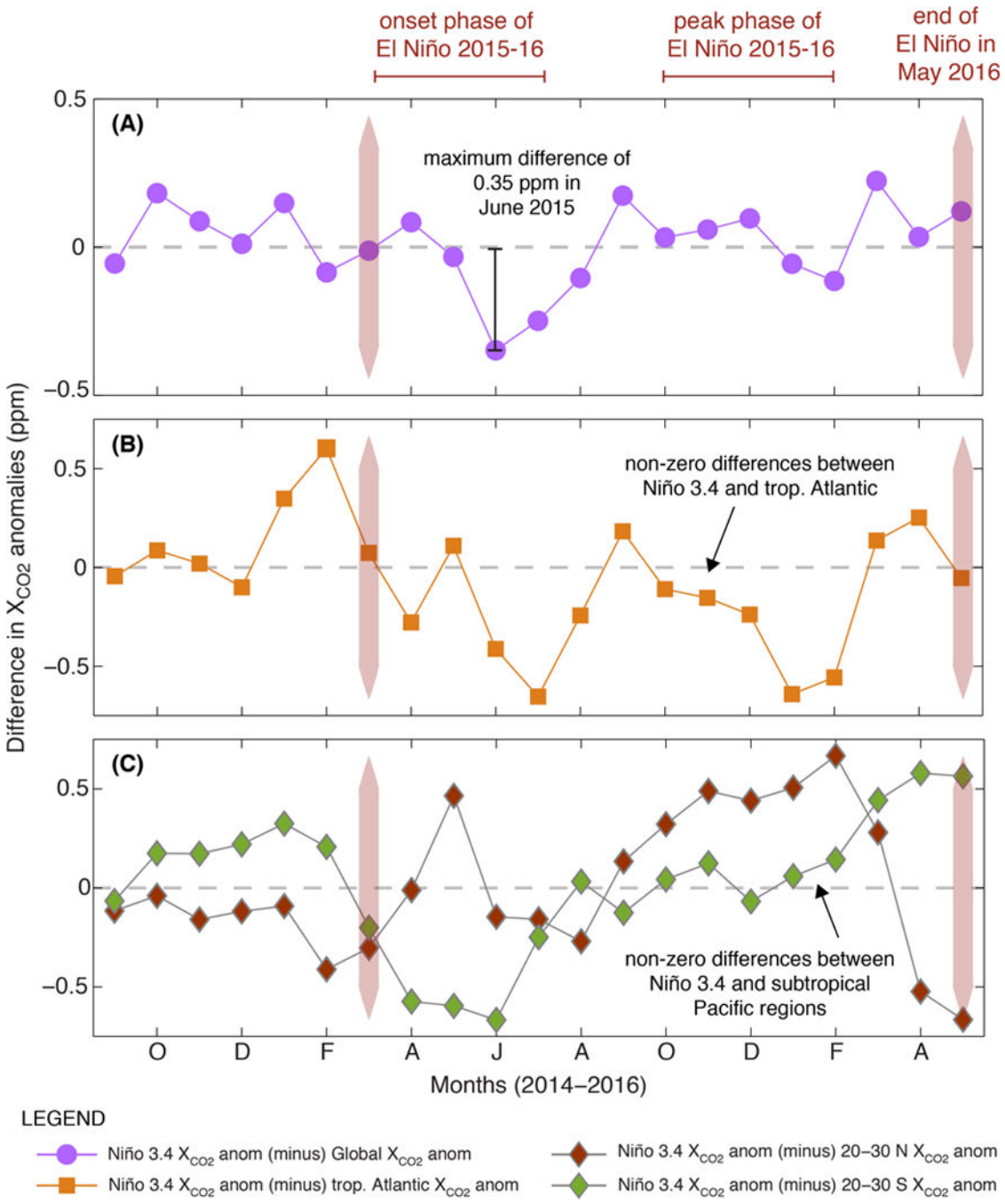

Fig. 4.

Difference in X_{CO2} anomalies between the Niño 3.4 region and (A) the globe, (B) the tropical Atlantic Ocean, (C) the subtropical Pacific Ocean from September 2014 to May 2016. Definitions of the regions are provided in Fig. 3. In Panel (A), we see a robust pattern of negative X_{CO2} anomaly between Niño 3.4 and the globe that is largest in 2015 and well synchronized with the onset phase of El Niño. In Panels (B) and (C), non-zero differences between Niño 3.4 and the other ocean basins indicate that the Niño 3.4 trend is not

reproducible in other ocean basins; thus, allowing us to attribute the negative anomaly in Fig. 2B to a reduction in local CO_2 outgassing over the tropical Pacific Ocean.

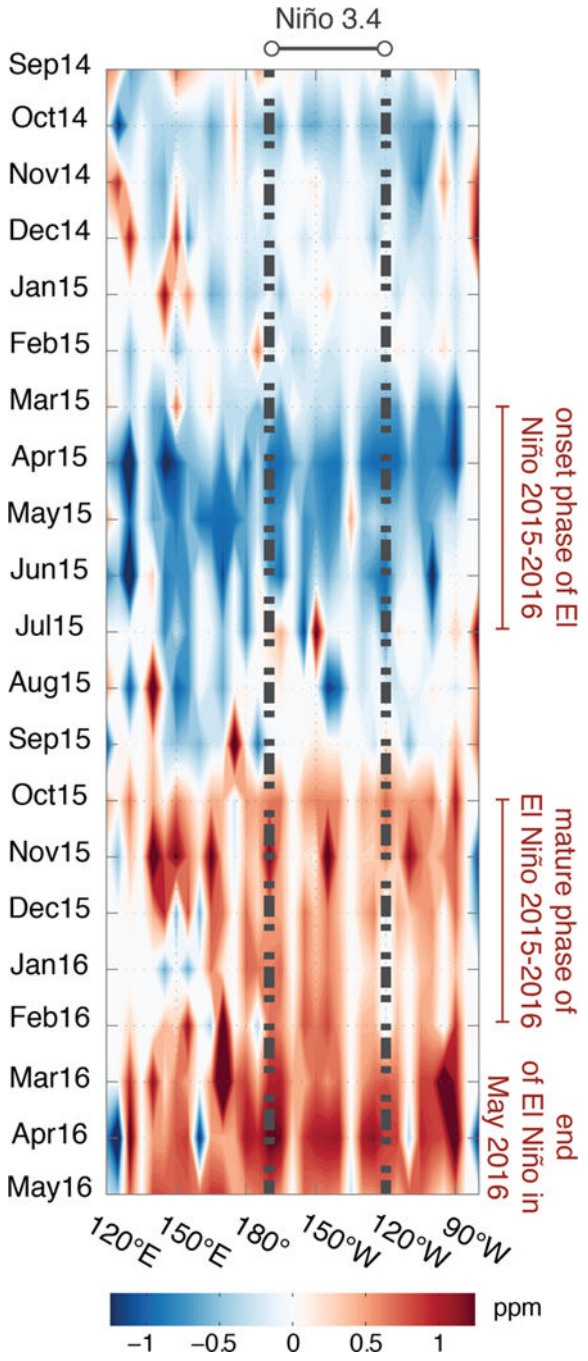

Fig. 5.

Time evolution of the X_{CO2} anomalies (ppm) averaged over 5°S–5°N. The x-axis represents longitude and the y-axis shows the time progressing from top to bottom in months. The 2015–2016 El Niño event and its onset and mature phases are highlighted to show the distinct responses observed over the tropical Pacific Ocean. The grey dashed lines capture the boundaries of the Niño 3.4 region. During the onset phase (i.e., March – July 2015), perceptible gradients are observable from the far western Pacific to the central Pacific (consistent with the increasing flux from west to east) along with high variability in the

X_{CO2} anomalies in the central Pacific. We also notice that the X_{CO2} anomalies are smaller over the eastern Pacific, which is consistent with surface seawater pCO_2 data collected on the TAO buoys (92). The transition from the ocean to the terrestrial signal happens between July and October 2015. Towards the latter stages of the El Niño event (i.e., November 2015 and later), the terrestrial signal dominates the observed trends in X_{CO2} likely masking any underlying ocean signal.